Chinese Chemical Letters 35 (2024) 109622

Contents lists available at ScienceDirect

Chinese Chemical Letters

journal homepage: www.elsevier.com/locate/cclet

Recent advances in near infrared (NIR) electrochemiluminescence luminophores

Yuyang Zhou [a,b,*], Ziwang Mao [b], Jing-Juan Xu [a,*]

[a] State Key Laboratory of Analytical Chemistry for Life Science, School of Chemistry and Chemical Engineering, Nanjing University, Nanjing 210023, China
[b] School of Chemistry and Life Sciences, Suzhou University of Science and Technology, Suzhou 215009, China

ARTICLE INFO

Article history:
Received 1 September 2023
Revised 15 January 2024
Accepted 8 February 2024
Available online 14 February 2024

Keywords:
Electrochemiluminescence
NIR
Luminophore
Nanocluster
Metal complex

ABSTRACT

Electrochemiluminescence has been developed as a robust analytical technique owing to its intrinsic advantages, such as near-zero background signal noise, wide dynamic ranges, high sensitivity and low cost and simple equipment. ECL luminophore as the critical component to generate light signals plays significant roles in this robust analytical system. Compared with traditional ECL luminophores, near infrared (NIR) ECL luminophores have attracted significant attentions recently due to their negligible autofluorescence, lower background interference and deep tissue penetration. Although substantial progresses have been achieved in exploring novel NIR ECL luminophores and elucidating their roles in addressing diverse challenges, there is still scarce of comprehensive reviews on the development of NIR ECL luminophores so far. In this review, the recent advancements on NIR ECL materials, including inorganic metal complexes, organic small molecules, metal nanoclusters, quantum dots and lanthanide-based materials, have been thoroughly summarized and discussed. In addition, we also provide a comprehensive overview of the challenges and prospects that lie ahead for the future development of NIR ECL luminophores in the future.

1. Introduction

Electrochemiluminescence (ECL, also named electrogenerated chemiluminescence) is generated on electrode surface through a series of electrochemical and chemical reactions to produce excited states of luminophores. Unlike photoluminescence (PL), ECL is intrinsically free from the interferences of excitation light source. Currently, owing to its low signal/noise ratio, high sensitivity, wide dynamic ranges and low-cost equipment, ECL has been developed to one kind of robust and powerful analytical techniques in clinical diagnostics, biosensors, environmental and pharmaceutical analysis, *etc*.

Considering the critical roles in ECL assays, extensive studies have been focused on exploring new ECL luminophores in the past few decades. Compared with luminophores with visible emission, near-infrared (NIR, 650–1700 nm) ECL luminophores have many advantages, such as minimal absorption from biological media, deep tissue penetration, lower background interference, and reduced photochemical damage. Since the first report about heptamethine cyanine dye with NIR ECL emission in acetonitrile by the group of Bard in 1997 [1], NIR ECL emission from inorganic metal complex [2], quantum dots/nanocrystals [3], metal clusters [4] and others [5] are subsequently reported by researchers. Owing to their great potential advantages as mentioned above, NIR ECL luminophores as one kind of emerging "star" luminophores have received much attentions and achieved rapid progresses in the past few decades. Unfortunately, there are still very rare literatures to specially summarize the vigorous NIR ECL studies except only one review article about the development of quantum dots based NIR ECL written by Wang and Han in 2013 [6].

Herein, in order to look back the remarkable progresses about NIR ECL luminophores and guide the interested researchers on the trend, we detailed summarized the recent developments of NIR ECL luminophores and corresponding analytical applications in this review (Fig. 1). According to the composition, these reported NIR ECL luminophore are classified to inorganic metal complexes, organic small molecules, metallic nanoclusters, quantum dots/nanocrystals and lanthanide-based materials. In addition, the corresponding analytical applications and unsolved challenges relied on NIR ECL luminophores have also been summarized and discussed here. We envisaged this review could help the related researchers focusing on different kinds of luminophores to quickly

* Corresponding authors.
E-mail addresses: zhouyuyang@mail.usts.edu.cn (Y. Zhou), xujj@nju.edu.cn (J.-J. Xu).

https://doi.org/10.1016/j.cclet.2024.109622
1001-8417/

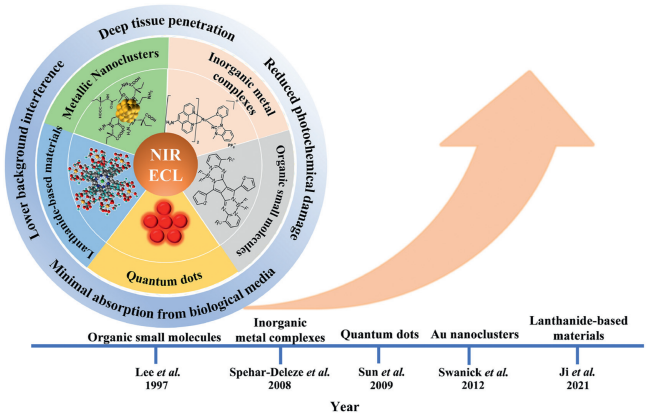

Fig. 1. The classifications, benefits, and time line of NIR ECL luminophores.

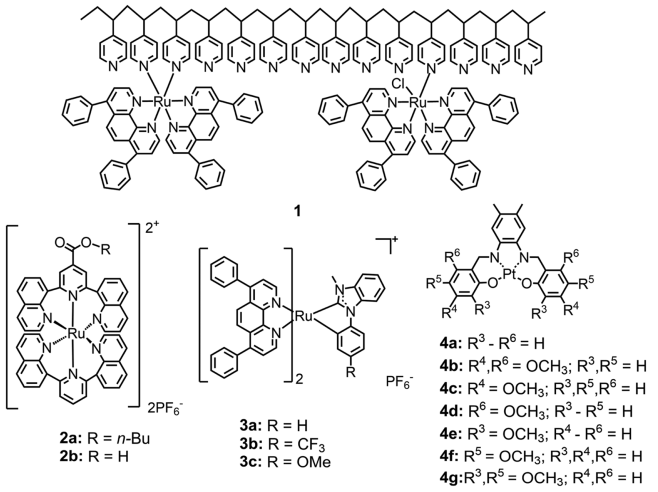

Fig. 2. Molecular structures of compounds **1**–**4**.

understand and acquire the whole current states of various kinds of NIR ECL luminophores, and promote the further developments of NIR ECL studies in the future.

2. NIR ECL luminophores

2.1. Inorganic metal complexes

As well-known, since the pioneering work by Tokel and Bard in the 1970s [7] and subsequently successfully used in the commercially clinical diagnostic products [8], tris(2,2′-bipyridine) ruthenium(II) and derivatives as the representative of inorganic metal complexes have become the most widely-used luminophores in the ECL-based analytical applications. However, though some studies have tried to improve ECL properties of ruthenium(II)-based *via* optimizing chemical structures of three bipyridine coordination ligands, such as incorporating substituents or increasing π conjugation of bipyridine, it is still very hard to largely tune emission colors of ruthenium complexes containing six Ru-N coordination bonds (abbreviated as RuN6) due to intrinsic electronic fields between coordination ligands and ruthenium center [9]. In order to redshift the maximum emission wavelength of ruthenium-based luminophores into NIR regions, one strategy is to exchange one Ru-N bond with Ru-Cl and new obtained complex RuN5Cl usually would have much larger wavelength compared with RuN6. However, the quantum efficiency of RuN5Cl decreased 10–20 folds compared with the traditional RuN6 complexes [9], which intensely hindered its luminescent applications. In 2008, the group of Robert J. Forster [2,10] ingeniously constructed the energy transfer pathways from RuN6 to RuN5Cl through incorporating RuN6 and RuN5Cl simultaneously into one poly(4-vinylpyridine) backbone (PVP) backbone (compound **1**, Fig. 2). Two emission centers named $[Ru(dpp)_2]^{2+}$ and $[Ru(dpp)_2Cl]^{+}$ (dpp is 4,7-diphenyl-1,10-phenanthroline, having much large π degree compared with bipyridine) are selected as the representatives of RuN6 and RuN5Cl respectively and incorporated into PVP backbone through the coordination bonds between ruthenium center and N atoms in pyridine unit of PVP polymer. This metallopolymer exhibited only one single PL emission band at 720 nm in aqueous solution or thin films, indicating the energy transfer from RuN5 to RuN5Cl moiety is efficient on this condition. Significantly, using sodium oxalate as co-reactant, the metallopolymer thin film on fluorine-doped tin oxide electrodes (FTO) could generated NIR emission centered at 720 nm, this is the first report about ruthenium-based NIR ECL luminophore. The cyclic voltammetry and ECL studies demonstrated RuN6 is firstly oxidized electrochemically and subsequently react with oxalate, the following formed excited states of $RuN6^{2+*}$ is further transferred to RuN5Cl center rather than directly decaying to the ground state of RuN6. Herein, the following energy transfer induced NIR ECL mechanism has been illustrated as following (Eqs. 1–6) [10]:

$$RuN6^{2+} - e^{-} \rightarrow RuN6^{3+} \quad (1)$$

$$RuN6^{3+} + C_2O_4^{2-} \rightarrow RuN6^{2+} + C_2O_4^{\bullet -} \quad (2)$$

$$C_2O_4^{\bullet -} \rightarrow CO_2^{\bullet -} + CO_2 \quad (3)$$

$$RuN6^{3+} + CO_2^{\bullet -} \rightarrow RuN6^{2+*} + CO_2 \quad (4)$$

$$RuN6^{2+*} + RuN5Cl^{+} \rightarrow RuN6^{2+} + RuN5Cl^{+*} \quad (5)$$

$$RuN5Cl^{+*} \rightarrow RuN5Cl^{+} + h\nu\ (720\,nm) \quad (6)$$

It should be noted the aforementioned such energy transfer is just limited to the condition of aqueous solution and thin films [2,10]. In contrast, two PL peaks according to RuN6 and RuN5Cl respectively would be observed in organic solution, indicating these two emission centers on PVP backbone communicate weakly in organic solution [2]. Furthermore, as for RuN5Cl with the coordination mode of $[Ru(N^N)_2NCl]^{+}$, it still has much more closer relationships with the π conjugation degree of N^N bidentate ligand rather than N monodentate ligand in tuning emission colors [11].

More recently, D'Alton *et al.* [12] synthesized bimetallic polymer with three emission centres by a single-step modification of $[Ru(bpy)_2PVP_{10}]^{2+}$ (bpy = bipyridine, PVP = poly-4-vinylpyridine) with iridium precursor (Fig. S1 in Supporting information). Importantly, the addition of increasing equivalents of iridium to the ruthenium center in the monometallic ruthenium polymers significantly enhanced the intensity of ECL emission. Consequently, this improvement led to a lower detection limit for the co-reactant oxalate from 20 μmol/L to 5 μmol/L. These findings could be attributed to the highly efficient energy transfer from iridium to ruthenium centers within the polymer layer after electrochemical excitation (ECL-ET). This phenomenon facilitates facile modification of ECL-active metal polymers with enhanced ECL activity, thereby introducing novel photoluminescence properties and further enhancing ECL emission.

Another type of ruthenium-based NIR ECL luminophore has been reported by Majuran and coworkers in 2020 [13]. These NIR ruthenium complexes (**2a** and **2b** in Fig. 2) have two N^N^N tridentate ligands and the ECL peaks of **2a** and **2b** located at 710 nm

and 715 nm, respectively. Furthermore, **2a** with *n*–butyl ester substituent has much higher ECL efficiency compared with **2b** with corresponding carboxylic group due to much more favorable reversible reductive potential of **2a**. Though the ECL efficiencies are still much lower than that of the standard reference of $Ru(bpy)_3^{2+}$, these heteroleptic $[Ru(N^N^N)_2]^{2+}$ could effectively facilitate an attachment point for further bioconjugation studies in the real ECL sensing applications in the future.

Recently, we [14] incorporated N-heterocyclic carbene (NHC) ligand (C*^C) into ruthenium complexes and successfully synthesized three NHC-based ruthenium complexes (RuNHC) with formula of $Ru(N^N)_2(C^*^C)^+$ (**3a**, **3b**). The electrochemical and ECL studies demonstrated that the substitution of one N^N ligand with C*^C bidentate ligand not only induced much lower oxidation potential of ruthenium(II) complex, but also redshift the emission of ruthenium complex into NIR regions. Considering that the degree of ligand conjugation plays a crucial role in regulating the emission wavelength of the corresponding metal complex, we selected 4,7-diphenyl-1,10-phenanthroline (DIP) as the N^N coordination ligand due to its large degree of conjugation. Additionally, *N*-methyl-*N*′-phenyl-benzo[*d*]imidazolium and its derivatives were chosen as C^C* ligands. Most importantly, these three RuNHC complexes exhibited much higher, or at least comparable ECL efficiency than $Ru(bpy)_3^{2+}$ under the same experimental conditions. Furthermore, the carbon anion in C*^C bidentate ligands also decrease the charge of the main motif of ruthenium complexes, which may have much smaller effects on biomolecules in the further bioconjugation applications. In conclusion, the advantages of longer wavelength (over 800 nm), higher ECL efficiency, low oxidation potential and charges of main motif would prove these great potential applications of these $Ru(N^N)_2(C^*^C)^+$ in NIR ECL-based analytical techniques.

Apart from ruthenium complexes, Reid *et al*. have also synthesized and investigated the photophysical and ECL properties of a series of platinum(II) Schiff base complexes (**4a**-**4g**). Among them, two platinum complexes with one methoxy substituent *para* to the oxygen on Schiff ligands (**4f**) and two methoxy substituent *para* and *ortho* to the oxygen on Schiff ligands (**4g**) exhibited NIR emission with peaks located at 696 nm and 739 nm. Using tripropylamine (TPrA) as co-reactant, the ECL efficiency of **4f** is up to 35.6% compared with the reference of $Ru(bpy)_3^{2+}$ ($\Phi_{ecl} = 100\%$) in dichloromethane solution, which is best ECL efficiency between **4f** and **4g** both in annihilation and co-reactant pathways. Though the efficiency of these two platinum NIR ECL luminophores is not very satisfactory, a wide range of wavelengths by small and easily implemented changes to Schiff based ligand structure is indeed unsurpassed in ECL systems, especially for further designing NIR ECL luminophores in the future.

Finally, though there are much more kinds of metal complexes-based NIR luminophores beyond the above-mentioned chemical structures, the reports about photoluminescent properties rather than ECL-related properties and applications do not fall into the scope of this review focusing on NIR-based ECL luminophores. Meanwhile, because the excited states generated from photoluminescence and ECL are usually identical to each other, metal complexes-based NIR ECL luminophores still have tremendous prospects of development in the future.

2.2. Organic small molecules

The first report about organic small molecular-based NIR luminophore is heptamethine cyanine dye 2-[4′–chloro-7′-(1′′-methyl-3′′,3′′-dimethylindolin-2′′-ylidene)3′,5′-(propane-1′′′,3′′′-diyl)-1′,3′,5′-heptatrien-1′-yl]–1-methyl-3,3-dimethylindolinium cation (**5** in Fig. 3) reported by Bard group in 1997 [1]. In the presence of TPrA, **5** could generate NIR emission centered at

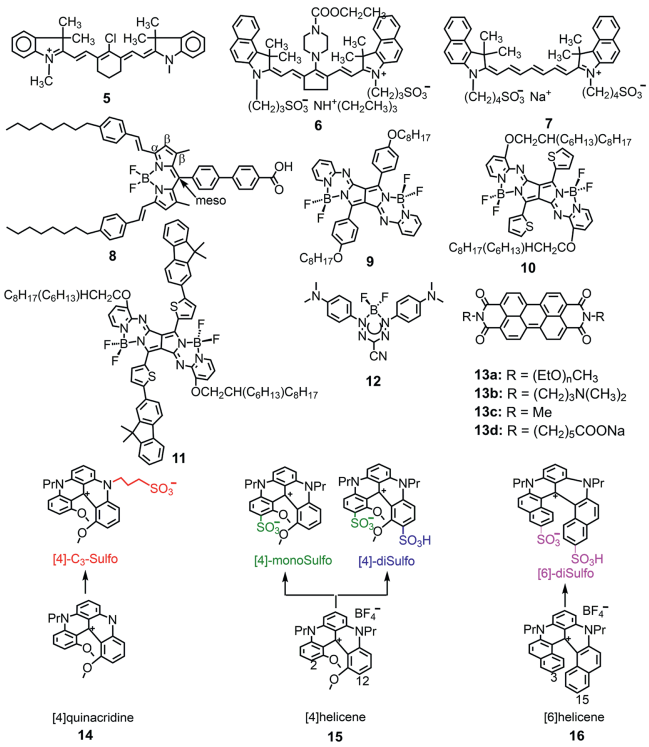

Fig. 3. Molecular structures of compounds **5**–**16**.

805 nm along with the oxidation potential over 0.7 V *vs.* SCE in acetonitrile solution and the corresponding ECL efficiency is 21% compared with $Ru(bpy)_3^{2+}$ as standard. Meanwhile, another indocyanine dye (**6**) has also been reported as an efficient NIR ECL luminophore by the same group in 1998 [15]. It has maximum ECL wavelength centered at 825 nm and the ECL efficiency of **6** with TPrA as co-reactant is 0.17 compared with $Ru(bpy)_3^{2+}$ as standard. It should be emphasized that micelle system containing sodium dodecyl sulfate surfactant has been verified as a new efficient ECL reaction solution for hydrophobic luminophores in this study. Notably, though another cyanine analogue (**7**) [15] in the same work has also exhibited NIR emission, it has very weak ECL efficiency compared with **6** due to the conformationally rigid polymethine chain in **7**. Overall, these cyanine dyes pioneeringly opened the research fields of exploring NIR-based ECL luminophores.

Beside cyanine-based organic small molecular luminophore, the boron-dipyrromethene (BODIPY, abbreviated as BDY) dye family is another kind of important luminophores with various applications, including NIR ECL fields. Bard and co-workers pioneered the study of various BDY dyes as ECL emitters, demonstrating that the structural properties significantly influence both the wavelength and efficiency of ECL emission [16]. In 2015, Ding group first investigated the ECL properties of one kind of BDY-1 dye (**8**) [17]. Its blocking units at alpha, beta or *meso* positions of BDY-1 core was deliberately selected to stabilize its radicals and improve ECL efficiency accordingly. The spooling ECL spectra of **8** with TPrA as co-reactant displayed a peak emission at 707 nm ascribed to intermolecular transitions. Most importantly, this kind of luminophore could reach an efficiency as high as 100% relative to $Ru(bpy)_3^{2+}$ at a low potential scan rate of 20 mV/s, demonstrating the feasibility of BDY as an efficient dye for ECL applications. In addition, Ishimatsu *et al*. also reported three pyrrolopyrrole aza-BODIPYs (**9**–**11**) with efficient NIR ECL properties using TPrA as co-reactant [18]. All these three BDY-based NIR luminophores displayed maximum ECL wavelength centered over 650 nm and the peak wavelength of **11** is even up to 777 nm. Most importantly, kinetic analysis of these

PPABs based on Marcus theory indicates the direct formation of S2 and T2 states through the electron transfer reaction, which would increase its ECL efficiency accordingly. The new insights about excited states formation of low energy dyes give us inspirations to develop high efficiency NIR-based luminophores in the future.

Another organic small molecular NIR ECL dye reported is boron difluoride formazanate (**12**) [19]. Compared with the former cyanine and BDY dye located at around 800 nm, the ECL wavelength of this kind luminophore redshift to 910 nm, which is the largest wavelength among these organic small molecular-based NIR ECL luminophores reported so far. Another advantage for this kind luminophore is that its chemical structure is very simple, which would avoid from laborious synthetic processes.

Perylene diimide (PDI) derivatives are another kind of important luminescent small molecular materials due to their intense and high quantum efficiency. Large conjugation degree and rigid structure from the perylene-skeleton with many aromatic rings is the "rapier": One side it indeed makes the wavelength of these luminophores redshift to NIR regions, while it also inevitably induces the disturbing drawbacks of poor solubilities in common solvents. In 1998, Williams *et al.* first reported the voltammetric and ECL properties of a class of PDI derivatives (**13a**), in which two oligomeric polyether chains are covalently linked to the perylene moiety *via* imide groups [20]. The cathodic ECL of these PDI polyether hybrids assisted by $S_2O_8^{2-}$ have well been investigated in this work. It should be noted that though their solubilities have been improved through polyethylene functionalized, the major peak wavelength of these derivatives in dilute solution are still lower than 600 nm though the shoulder peak of I-550 located at 625 nm. Recently, the group of Wang in Liaocheng University further explored a series of PDI-based ECL luminophores (**13b**-**13d**). Encouragingly, all these PDI-based luminophores displayed NIR ECL centered at *ca.* 700 nm with a very lower cathodic potential. Combining with graphene oxide (GO) and gold nanoparticles (AuNPs), the single cathodic/both cathodic and anodic dual ECL immunosensors to sensitively detect CEA and AFP has well been constructed [21–23].

Very recently, Sojic *et al.* also synthesized sulfonate substituted helicenes as aqueous soluble NIR luminophores (**14**–**16** in Fig. 3) [24–27]. As expected, these sulfonate derivatives have much better water solubilities compared with its parent skeletons. Furthermore, incorporating sulfonate group also induced emission wavelength up to 708 nm for the compound of [4]-diSulfo. The corresponding ECL efficiencies ranged from 5.4% to 33.9% using $Ru(bpy)_3^{2+}$ as standard ($\Phi_{ecl} = 100\%$).

Overall, it is easy to find that large conjugated aromatic rings and rigid planar skeleton are usually indispensable to tune the emission into NIR regions as for pure organic small molecular. Poor solubility and laborious synthetic works may be the two unignorable obstacles to hinder the developments of this kind of NIR luminophores in the future.

2.3. Metallic Nanoclusters

Metal nanoclusters are composed of a few to several hundred metal atoms and protective ligands, with particle sizes close to the Fermi wavelength of electrons (typically less than 2 nm). These clusters exhibit discontinuous electronic energy levels, possess molecular-like properties, and have the ability to generate electrochemiluminescence. The luminescent characteristics of metal nanoclusters are influenced by various factors including size, ligand composition, number of metal atom species, and valence state [28]. Generally, the electrochemiluminescence spectra of metal nanoclusters display a red-shift compared to photoluminescence and can extend into the near-infrared region. Due to their exceptional electrochemical and optical properties, favorable biocompatibility, as well as facile surface modification capabilities, there is significant research interest in developing metal nanoclusters that emit near-infrared electrochemiluminescence.

The NIR-ECL emission based on Au nanoclusters (AuNCs) was first reported by Ding and his coworkers, who investigated the ECL of organic-soluble $Au_{25}^{z}(SR)_{18}$ ($z = 1+, 1-, 0$) [4,29,30], $Au_{144}(SR)_{60}$ [31] and $Au_{38}(SR)_{24}$ [32] nanoclusters (SR = 2-phenylethanethiol) under various conditions. The first report about AuNCs-based NIR-ECL emission is the compound of $Au_{25}(SR)_{18}^{+}$ [4]. Its detailed NIR emission mechanism including annihilation and co-reactant pathways is unprecedently revealed by the group of Ding through the techniques of electrochemistry, NIR PL spectroscopy combined with their developed spooling ECL spectroscopy. The weaker NIR ECL of Au_{25} was observed during the annihilation process of electrically generated Au_{25}^{2+} and Au_{25}^{2-}, while the intensity of NIR ECL was enhanced with the assistance of benzoyl peroxide (BPO) as reductive-oxidation co-reactant. The ECL process could be presented as follows (Eqs. 7–10):

$$BPO + e^- \rightarrow BPO^{-\bullet} \quad (7)$$

$$BPO^{-\bullet} \rightarrow C_6H_5CO_2^{\bullet} + C_6H_5CO_2^{-} \quad (8)$$

$$C_6H_5CO_2^{\bullet} + Au^- \rightarrow Au_{25}^0 + C_6H_5CO_2^{-} \quad (9)$$

$$Au_{25}^0 + BPO^{-\bullet} \rightarrow Au_{25}^{-*} + BPO \quad (10)$$

Subsequently, Ding and co-workers in the study of $Au_{25}(SR)_{18}^{-}$ revealed that the ECL mechanism can be achieved more effectively in the presence of TPrA and BPO as co-reactants [29]. The redox states of Au_{25}^{-} precursor were readily accessible, and the Au_{25}^{-}/BPO co-reactant system shows greater favorability compared to its corresponding Au_{25}^{+}/BPO counterpart. The subsequent investigations revealed that Au_{25}^{0} clusters exhibit enhanced susceptibility to undergo oxidation–reduction reactions, leading to the generation of more stronger NIR ECL signals in the presence of TPrA and under specific trigger voltages [30]. They also revealed the thermodynamic relationship between the five oxidation states of Au_{25} (Au_{25}^{2+}, Au_{25}^{+}, Au_{25}^{0}, Au_{25}^{-}, and Au_{25}^{2-}) and the three excited states in their summary (Fig. S2 in Supporting information) [33]. Considering the more abundant number of attainable redox states within the potential range, Ding and co-workers synthesized monodisperse $Au_{144}(SR)_{60}$ by investigating the adjustment of the gold to 2-phenylethanethiol synthesis ratio [31]. The ECL of Au_{144} was investigated through both annihilation and co-reactant pathways, with a focus on elucidating the mechanism underlying ECL generation *via* the co-reactant pathway. The NIR ECL of the $Au_{144}(SR)_{60}$ was observed, exhibiting a peak wavelength at 930 nm, in the presence of TPrA as the co-reactant. In order to gain insights into the impact of gold cluster core size on the wavelength, intensity, and efficiency of ECL, Ding *et al.* [32] successfully obtained near-infrared ECL from $Au_{38}(SR)_{24}$. The experimental results demonstrated that $Au_{38}(SR)_{24}$ exhibited significantly enhanced ECL at 930 nm when TPrA or BPO are employed as co-reactants. Recently, the significance of Au's valence state in enhancing the performance of ECL has been corroborated by other research groups through their investigations on AuNCs. Peng *et al.* [34] concluded that the electrochemical reduction of AuNCs depends on the reduction potential and that the enhancement of the ECL signal positively correlates with the reduction of AuNCs, suggesting that the valence state of gold plays a crucial role in the ECL performance of AuNCs.

For enhanced utilization of the bioanalytical capability of AuNCs, Wang *et al.* [35] first reported the NIR ECL of aqueous soluble lipoic acid Au NCs. This was achieved by covalently combining the redox-active gold clusters with *N*,*N*-diethylethylenediamine

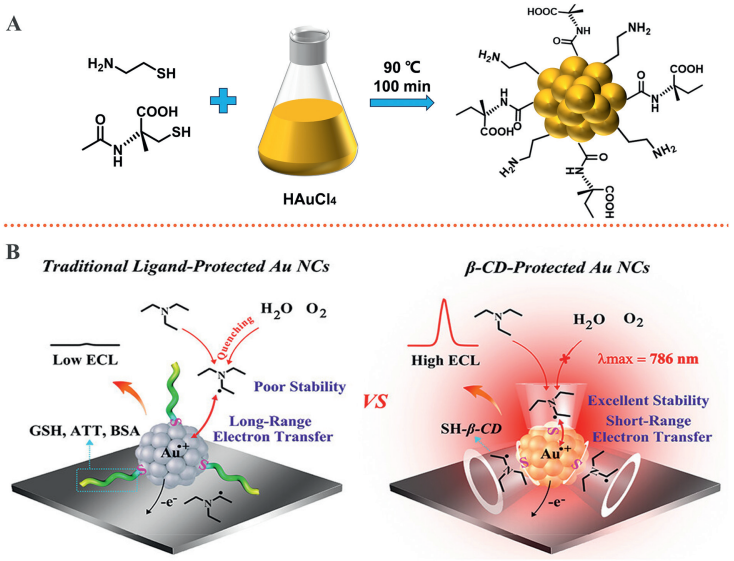

Fig. 4. (A) Preparation of NAC/Cys-AuNC. (B) Comparison of Traditional Ligand-Protected AuNCs (Left Panel) and the β-CD Protected Au NCs with a ligand-based shielding effect (right panel). Adopted with permission [41]. Copyright 2023, American Chemical Society.

(DEDA) (Fig. S3 in Supporting information). In terms of oxidative-reduction ECL generation, AuNCs exhibited superior efficiency compared to the standard $Ru(bpy)_3^{2+}$ in the presence of a high excess of TPrA, with an onset potential of 0.78 V. Consequently, further research endeavors were undertaken to reduce the high triggering potential of AuNCs and enhance the ECL. Meanwhile, Kim *et al.* [36] exploited the difference in the wavelength regions of PL and ECL to explore the potential information about the origin of ECL in orange fluorescent AuNCs. Water-soluble Au NCs were synthesized using glutathione (GS) as a reducing and stabilizing agent. The study confirmed that the near-infrared ECL in AuNCs was mainly caused by Au(0)-thiolate motifs through spooling ECL spectroscopy and time-resolved optical measurements. This further contributes to the understanding of water-soluble AuNCs.

Considering that small molecule ligands, when employed as stabilizers for AuNCs, not only broaden the wavelength range into the near-infrared region but also enhance the aqueous solubility of AuNCs. Peng *et al.* [37] employed small molecule ligands to synthesize Methionine-stabilized AuNCs (Met-AuNCs), utilizing methionine as both a reducing and stabilizing agent. Additionally, the electrodes were pre-oxidized with triethylamine (TEA) as a co-reactant, resulting in an impressive 66% ECL quantum luminescence efficiency achieved at *ca.* 800 nm under significantly reduced potential conditions. Subsequently, to further enhance the redshift of NIR ECL, Yu *et al.* [38] employed Met-AuNCs as the luminophore and triethanolamine (TEOA) as the co-reactant to achieve highly efficient ECL in an aqueous solution at 835 nm. Ju *et al.* [39] demonstrated a dual stabilizer capping strategy employing *N*-acetyl-L-cysteine and cysteamine as model capping agents for the synthesis of AuNCs (NAC/Cys-AuNCs) (Fig. 4A). This approach not only achieved remarkable performance in NIR ECL emission, but also improved water solubility and biocompatibility, resulting in a red shift of the ECL emission wavelength to 860 nm. Recently, Peng *et al.* [40] have reported an energy level engineering strategy to modulate ECL performance based on ligand-protected AuNCs as luminophores. By utilizing *N*,*N*-diisopropylethylamine (DIPEA) as a co-reactant, the energy level matching with AuNCs effectively enhances their electron transfer reactions, leading to the achievement of highly stable ECL signals with low trigger potentials. Yuan *et al.* [41] utilized the ligand-based shielding effect and employed β-cyclodextrin-protected AuNCs (β-CD-AuNCs) as luminophores to enhance the stability of co-reactant radicals, thereby achieving efficient ECL (Fig. 4B). This study elucidated the pivotal role played by ligands in augmenting the stability of active co-reactant radicals.

Introducing a core reaction accelerator can significantly enhance the ECL efficiency of AuNCs. Yuan [42] and Jia [43] introduced Pd@CuO and Cu_2S as co-reactant accelerators, respectively, to form a ternary system with bovine serum albumin-templated AuNCs (BSA-AuNCs) for constructing an ECL immunosensor. This approach significantly enhanced the ECL luminescence efficiency. Recently Ju group [44] successfully fabricated a hollow double-shell structure $CuCo_2O_4$@Cu_2O(HDS-$CuCo_2O_4$@Cu_2O) heterostructure for the first time and employed it as an efficient co-reactant triisopropanolamine (TPIA) accelerator to enhance the NIR ECL performance of Au NCs (Fig. S4 in Supporting information). The resulting heterojunction offers a reduced charge transfer distance, enhanced interface charge transfer efficiency, and improved separation capability, thereby significantly promoting the generation of abundant co-reactant intermediate radicals and cationic radicals of AuNCs to achieve nearly threefold stronger near-infrared ECL response compared to individual AuNCs. Then, a probable mechanism of the NIR ECL immunosensor was exhibited as follows (Eqs. 11–15):

$$AuNCs - e^- \rightarrow AuNCs^{+\bullet} \quad (11)$$

$$TPIA + h^+ \rightarrow (HDS - CuCo_2O_4@Cu_2O)TPIA^{\bullet+} \ (more) \quad (12)$$

$$TPIA^{\bullet+} \rightarrow TPIA^{\bullet} + H^+ \quad (13)$$

$$AuNCs^{+\bullet} + TPIA^{\bullet} \rightarrow AuNCs^* \quad (14)$$

$$AuNCs^* \rightarrow AuNCs + h\nu \ (830\,nm) \quad (15)$$

Furthermore, other reports have also highlighted the utilization of other types of metal nanoclusters. Shen *et al.* [45] investigated silver nanoclusters (AgNCs) that exhibit exceptional near-infrared ECL in aqueous solutions. The synthesized bovine serum albumin-stabilized silver nanoclusters (BSA-AgNCs) displayed a strong anodic ECL peak at 904 nm with triethanolamine (TEtOA) as a co-reactant, and their superior NIR ECL performance was utilized for

spectral-resolved tricolor ECL multiplex immunoassay (MIA). By combining with two other visible light-labeled probes as ECL labels, simultaneous detection and identification of multiple target analytes can be achieved. The growing interest in copper nanoclusters (CuNCs) has been observed in recent years. Lv [46] reported a one-pot wet chemical reduction method for preparing bright, NIR CuNCs. In the presence of $K_2S_2O_8$, the ECL exhibited its maximum intensity at 735 nm, representing a red shift of at least 135 nm compared to other types of CuNCs. A sandwich-type ECL immunosensor fabricated using this material successfully detected real human serum samples without employing any signal amplification strategies.

More significantly, it has been demonstrated that the synergistic interactions among metallic elements result in an augmented ECL response [47]. Chen [48] proposed the integration of co-reactant functionality into ligand monolayers *via* covalent coupling, thereby simplifying the charge transfer process to an intracluster mechanism. This study reports a rod-shaped bimetallic $Au_{12}Ag_{13}$ nanocluster that obtained an ECL emission wavelength of 775 nm in annihilation mode, which is 10 times stronger than that of $Ru(bpy)_3^{2+}$ and 400 times stronger than that in co-reactant mode. The strong ECL of $Au_{12}Ag_{13}$ originates from the 13^{th} Ag atom located at the central position, which stabilizes the charge on the LUMO orbital and enhances the stability of the rod-shaped $Au_{12}Ag_{13}$ nucleus. Fu *et al.* [49] have reported a bimetallic nanocluster consisting of Au and Ag, which was synthesized through the introduction of Ag into AuNCs. This particular nanocluster demonstrates remarkable single-band ECL efficiency in aqueous environments, exhibiting a maximum emission wavelength of approximately 906 nm. Moreover, it has been successfully employed for spectroscopy-based quantitative ECL bioanalysis within the NIR-II region. Further, Ju *et al.* [50] employed an ion-doping strategy to modulate the ECL emission of Au NCs, enhancing their emission efficiency by doping with Co^{2+}. This approach generated tunable hole injection channels for ECL emission and reduced surface defects through the synergistic effect of Au and Co^{2+}, promoting electron transfer. The resulting Co^{2+}-AuNCs exhibited reduced trigger potentials, twice the ECL efficiency and intensity of AuNCs, with ECL emission occurring at 820 nm (Fig. S5 in Supporting information).

2.4. Quantum dots/nanocrystals

Quantum dots (QDs, also named nanocrystals) are composed of semiconductor materials with adjustable physical dimensions and distinctive photoelectric properties. As a novel class of inorganic luminescent dyes, QDs have also attracted great attentions and demonstrated huge potential applications in wide fields [51–53]. Since the first study about the ECL behavior of silicon QDs in 2002 [54], QDs have been extensively studied as a new type of ECL material. Notably, owing to their size/surface-dependent tunable luminescence, QDs also exhibit great promising prospects as NIR ECL emitters in the recent years [6,55,56]. It should be noted that this subsection highlights the research advancements in NIR ECL QDs over the past decade, particularly focusing on those NIR ECL QDs that offer innovative solutions to unresolved challenges in ECL.

In 2009, Sun and co-workers reported the generation of NIR ECL from PbS QDs in organic electrolyte solution for the first time, verifying the close connection between ECL and the surface chemistry of QDs (Fig. S6 in Supporting information) [3]. Subsequently, Wang *et al.* [57] reported the synthesis of CdTe/CdS/ZnS QDs and investigated the impact of the ZnS shell layer on NIR ECL properties, demonstrating a strong and stable ECL signal that was nine times higher than the maximum ECL emission intensity observed for CdTe/CdS QDs during cathodic scanning. Furthermore, employing cathodic scanning, Wang designed and reported a novel NIR ECL immunosensor by integrating QDs with nanomaterials to achieve signal amplification [58].

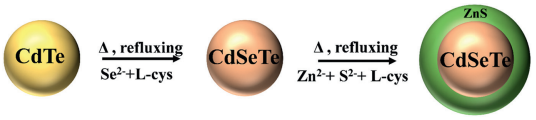

Fig. 5. Schematic illustration of the synthesis of water-soluble CdSeTe/ZnS CS QDs. Adopted with permission [65]. Copyright 2010, the Royal Society of Chemistry.

However, in the context of cathodic ECL, hydrogen peroxide generated through the electrochemical reduction of dissolved oxygen also acts as a cathodic ECL co-reactant, potentially leading to unforeseen interference. In a one-pot method, Zou and coworkers prepared CdTe QDs with highly efficient anodically enhanced NIR ECL using mercaptopropionic acid (MPA) and sodium hexametaphosphate (HMP) as capping agents [59,60]. Further, Zou *et al.* [61] also employed a one-pot synthesis method to fabricate dual-stabilized CdTe QDs, utilizing 2-(dibutylamino)ethanol (DBAE) as the reactant. Importantly, the as-prepared CdTe QDs, coated with dual stabilizers, were further utilized as near-infrared ECL labels for sandwich-type NIR ECL immunoassay. It should be noted that these NIR ECL CdTe QDs have been successfully employed to construct the spectra-resolved ECL immunoassays by Zou and co-works. For example, in 2017, they successfully developed a two-color ECL immunoassay for alpha fetoprotein (AFP) and carcinoembryonic antigen (CEA) by employing dual-stabilizer capped CdTe QDs (776 nm) and CdSe QDs (550 nm) as signal probes labeled on AFP and CEA antibodies respectively, along with the co-reactant $(NH_4)_2S_2O_8$ (Fig. S7A in Supporting information) [62]. Subsequently, the group further applied this CdTe QDs to construct triple color-resolved ECL multiplex immunoassay (Fig. S7B in Supporting information) [63]. These above studies demonstrated great advantages of NIR luminophores in spectra-resolved multiplex analytical applications. Notably, beside surface stabilization strategy, Co^{2+}has also been doped into CdTe QDs to red-shift its ECL wavelength into NIR windows by the same group [64].

As well-known, the presence of toxic ions such as Cd^{2+}, Pb^{2+} and Hg^{2+} is always one of un-negligible disadvantages of NIR QDs, which also restricts their applications in biomedical fields. To address this limitation, ZnS coatings are frequently employed to achieve core/shell nanostructures [56]. This approach not only enhances the biocompatibility of QDs, but also decreases surface defects, thereby improving their luminescent properties. Liang *et al.* [65] initially fabricated NIR ECL QDs by incorporating the ZnS shell layer on the core of CdSeTe for electrochemical luminescence, resulting in strong ECL and favorable biocompatibility (Fig. 5). Dennany *et al.* [66] also used 2-(dimethylamino) ethylene glycol (DAET) to modify CdSeTe/ZnS core-shell QDs and the as-prepared water-soluble NIR QDs with emission centered at 810 nm were further incorporated into a chitosan film for the development of an ECL biosensor to detect total cholesterol in blood. In addition, Wang *et al.* [67] investigated the anodic NIR ECL properties of 3-mercaptopropionic acid (MPA)-capped coated CdTe/CdS $core_{small}/shell_{thick}$ QDs in aqueous solution and developed them as a Cu^{2+} probe with low detection limit, sensitivity and selectivity. Furthermore, Wang and co-workers developed a novel ECL resonance energy transfer (ECL-RET) system utilizing MPA-capped CdTe/CdS core-shell quantum dots as highly emissive donors for ECL and gold nanorods (AuNRs) as efficient acceptors [68]. The sensitivity of this system towards thrombin detection was exceptional, achieving a remarkable detection limit of 31 amol/L (S/N = 3). Apart from the traditional QDs containing the element of Cd, Se and Te, Zou and co-workers further screened the ECL clusters to ensure the absence of toxic elements and assess their biocompati-

bility through an investigation of copper indium sulfide (CIS) QDs [69] and Ag-Ga-In-S (AGIS) QDs [70]. Yuan *et al.* [71] also used hydrothermal method to prepare alloyed silver gold sulfur QDs based NIR ECL emitters. Liu *et al.* [72] successfully synthesized biocompatible tetraphenylethylene nanocrystals (TPE NCs) through self-assembly of individual TPE molecules, leading to the observation of an aggregation-induced enhanced NIR ECL emission phenomenon. This discovery provided a robust ECL signal when triethylamine (TEA) is used as the co-reactant. These literatures provide some new avenues to develop environmental-friendly NIR ECL QDs in the future.

To achieve efficient ECL of QDs for bioanalysis, an intriguing strategy involving the integration of QDs with carbon nanomaterials such as MXene and graphene has also been reported. It could not only enhance the ECL intensity, but also mitigate the overpotentials in ECL systems. For example, Huan *et al.* [73] prepared CdTe QDs modified with multiwalled carbon nanotubes@reduced graphene nanoribbons (CdTe-WCNTs@rGONRs) composites based on electrostatic interactions, which resulted in a 4.5-fold increase in the ECL intensities and a decrease in the starting potential by 100 mV. Moreover, graphitic carbon nitride nanosheets (g-C_3N_4 NS) were also considered as efficient ECL emitter. Chang *et al.* [74] developed a highly sensitive and stable ECL immunosensor based on an innovative energy resonance transfer mechanism between NIR CdTe/CdS QDs and g-C_3N_4. This novel ECL system exhibited a wide linear range from 0.0001 U/mL to 10 U/mL, along with an impressively low detection limit of 0.034 U/mL for CA125 quantification. In addition, N–Ti_3C_2 MXene with oxygen-containing functional groups has also been used to red-shift the ECL spectra to NIR regions. Jiang *et al.* [75] prepared highly efficient NIR ECL materials, *i.e.*, well-dispersed AgBr QDs modified with Ti_3C_2 MXene nanocomposites (Ti_3C_2-AgBr QDs), using a simple wet-chemistry technique (Fig. S8 in Supporting information). Ti_3C_2-AgBr QDs exhibited ECL emission characteristics with adjustable wavelengths by changing the content of Ti_3C_2. Wei and co-workers also developed a one-pot method to fabricate a new novel efficient SnS_2 based NIR ECL QDs by decorating with Ti_3C_2 MXene nanocomposites (SnS_2 QDs-Ti_3C_2) [76]. Additionally, NIR AgBr-based QDs functionalized with nitrogen-doped Ti_3C_2 MXene nanocomposites have also been reported by Zhang *et al.* [77].

Apart from the above-mentioned semiconductor quantum dots containing metallic elements, another notable advancement in NIR ECL QDs is that nitrogen and sulfur-doped graphene quantum dots (GQDs) have also been developed as NIR ECL emitters by Ding's group recently [78]. The GQDs exhibited strong near-infrared (NIR) emission ranging from 680 nm to 870 nm when dispersed in an aqueous medium with $K_2S_2O_8$ as a co-reactant. We believe that much more kinds of novel low-toxicity NIR QDs would be explored in the future owing to the continuous advancement of both theoretical understanding and technological capabilities to precisely control the growth and manipulate the structures at nanoscale.

2.5. Lanthanide-based materials

Except the above traditional kinds of NIR ECL emitters, lanthanide-based emitters, known for their vibrant emission colors and exceptional luminescent properties, have emerged as promising NIR ECL materials in recent years [79]. In 2021, our group designed and synthesized a $NaYbF_4$@SiO_2 core–shell nanoparticle for the first time (Fig. 6A) [80]. The resultant materials exhibited NIR-II ECL emission center at 983 nm and have relative ECL efficiency as high as 383% in aqueous solutions. The detailed ECL mechanism characterized by DFT calculations and electrochemical data demonstrated that $NaYbF_4$ tended to be reduced to a relatively stable anion radical $NaYbF_4^{\bullet-}$, which subsequently reacted with $SO_4^{\bullet-}$ to generate an excited state. This work opens a new avenue to explore aqueous -soluble NIR-II ECL emitters.

Around the same time, the group of Wei in University of Jinan also investigated a series of Eu-based NIR ECL luminophores. In 2021, they firstly select 1,3,5-benzenetricarboxylic acid (H_3BTC) as

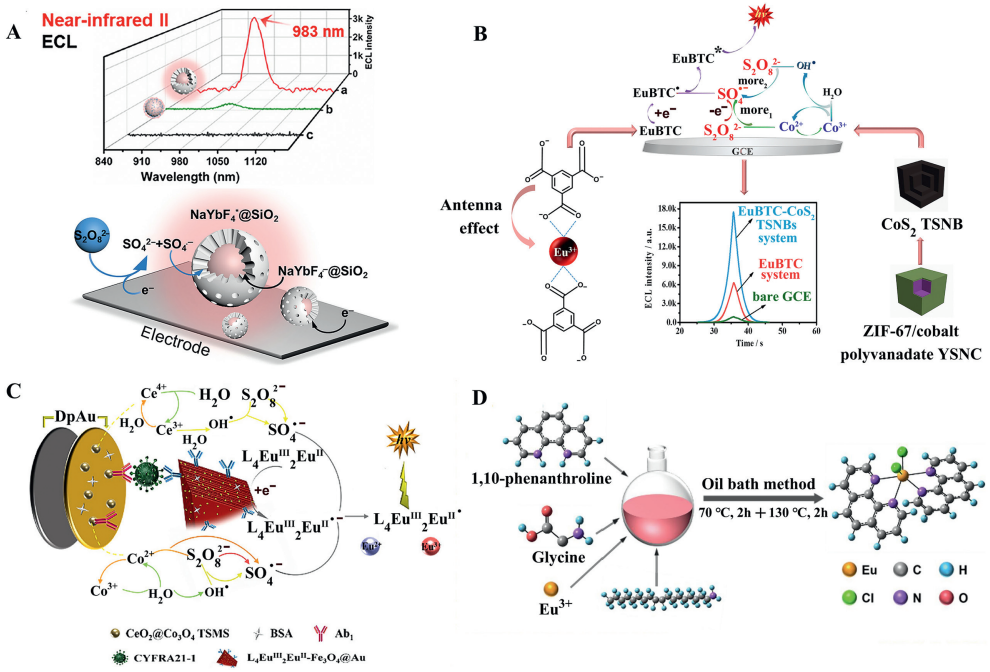

Fig. 6. (A) ECL spectra of $NaYbF_4$@SiO_2 (a, red), $NaYbF_4$ (b, green) modified GCE and bare GCE (c, black) in PBS solution with 100 mmol/L $K_2S_2O_8$ and schematic of the proposed ECL mechanism of $NaYbF_4$@SiO_2-$K_2S_2O_8$ system. Adopted with permission [80]. Copyright 2021, Chinese Chemical Society. (B) The mechanism illustration of the increased ECL by antenna effect and dual enhancement effect of CoS_2 TSNBs. Adopted with permission [81]. Copyright 2021, Elsevier. (C) The ECL biosensor fabrication and conjectural mechanism illustration in $K_2S_2O_8$ Adopted with permission [5]. Copyright 2021, American Chemical Society. (D) The synthesis route of Eu(II)-Phen. Adopted with permission [83]. Copyright 2022, Elsevier.

organic ligand and Eu^{2+} as metal ions to synthesize EuBTC metal-organic framework (MOF) (Fig. 6B) [81]. Due to strong antenna effect between Eu^{3+} and HBTC, this as-prepared EuBTC MOFs displayed strong NIR ECL emission centered at 880 nm under the assistant of co-reactant of $S_2O_8^{2-}$ and accelerators of CoS_2 hollow triple shelled nanoboxes (TSNBs). Furthermore, they successfully fabricated self-assembled sandwich-type biosensors based on this novel efficient NIR luminophore to sensitively detect procalcitonin. Afterwards, they [5] further prepared a mixed-valence trinuclear Ln-MOFs ($L_4Eu^{III}{}_2Eu^{II}$). Considering of $CeO_2@Co_3O_4$ three-shell microspheres (TSMS) co-reaction accelerator and the efficient antenna effect induced by the two coordination environment ligands in $L_4Eu^{III}{}_2Eu^{II}$, it demonstrated strong self-enhancement NIR ECL signals at approximately 900 nm and the following biosensors based on this novel luminophore also exhibited excellent performances (Fig. 6C). It should be noted that this novel mixed-valence Eu-MOF luminophore introduces a new member into the family of self-enhanced ECL materials. Combining this constructed biosensor based on NIR emitter, it would inevitably offer a promising approach for achieving efficient and sensitive ECL immunoassays.

Additionally, they also designed a Eu-MOF ($Eu_2[Ru(dcbpy)_3]_3$) with a novel annihilation electroluminescence mechanism [82]. The ligand $[Ru(H_2dcbpy)_3]\cdot Cl_2$ can undergo redox reaction to generate $Ru(dcbpy)^{3+/2+}$ pairs and then catalytically oxidize with $Eu_2[Ru(dcbpy)_3]_3$ to produce excited states of Eu-MOFs, which further decays to ground states *via* NIR emitting with 700 nm. In addition, the antenna effect would enhance ECL luminescence by transferring energy from $Eu_2[Ru(dcbpy)_3]_3\cdot Cl_2$ to the central metal ion. Finally, $Eu_2[Ru(dcbpy)_3]_3$ has been successfully employed as an efficient NIR ECL probe to sensitively detect trenbolone with LOD of 4.83 fg/mL.

Recently, Lu *et al.* [83] has also developed a novel Eu(II)-MOF (Eu(II)-Phen) as a new NIR probe to construct a high-sensitivity anode ECL sensor (Fig. 6D). In this report, glycine as a reducing agent and oleylamine as a protective agent were employed to obviate the need for excessive inert gas usage in order to prevent oxidation of Eu^{2+} to Eu^{3+}. The self-enhanced ECL mechanism of the sensor is achieved through utilization of the ligand's antenna effect on Eu^{2+}. Additionally, another self-enhanced ECL mechanism involves promotion of more rapid generation of TPrA radicals ($TPrA^{\bullet}$) catalyzed by Fe_3O_4-AgNRs. The dual self-enhancement mechanisms involving both the antenna effect of ligand on Eu^{2+} and catalytic effects from Fe_3O_4-AgNRs on TPrA serve to increase ECL intensity. Eu(II)-Phen in the above-mentioned work demonstrated significantly higher ECL efficiency compared to other luminophores such as $[Ru(bpy)_3]^{2+}$ and its derivatives with TPrA. The according NIR ECL sensor also exhibits good performances with low LOD of 4.42 fg/mL and wide linear ranges between 10 fg/mL $\sim$ 100 ng/mL.

In our opinion, though the development of lanthanide-based NIR ECL luminophores still stayed at its infancy stage currently, it has bright prospects in ECL-based analytical applications in the future owing to the exceptional ECL luminescent properties of lanthanide-based luminophores.

3. Conclusion and outlook

This review provides a comprehensive investigation into the development and current status of various kinds of NIR ECL luminophores, as well as their roles in addressing biological analysis applications. Noteworthy, despite continuous advancements of NIR ECL luminophores have been achieved in recent years, there are still challenges that require innovative and practical solutions.

(1) The current reported NIR luminophores usually lack labeling abilities, especially for inorganic metal complexes, organic small molecules and nanoclusters, which serious hinder their ECL-based analytical applications. Thus, developing new efficient NIR ECL luminophores with labelling abilities is highly desired in the future

(2) The ECL efficiency of most reported NIR luminophores are still relatively low, highly efficient NIR ECL luminophores are still urgently desired to improve the sensitivity of the following analytical applications in the future, which should be highly relied on optimizing the chemical structures of luminophores, such as increasing π-conjugation degree, incorporating substituents, tuning nano-structures, *etc.*

(3) Apart from the optimization of chemical structure of luminophore itself, it should be emphasized that exploring suitable co-reactant for NIR luminophores is also urgent desired to improve the overall ECL properties in the NIR ECL reaction systems taking into its crucial role in the generating ECL signals. For instance, when considering oxidative-reduction co-reactants, the correlation with NIR fluorescent materials can be estimated by employing the equation: $E_{red}(\text{co-reactant}^{\bullet}) < E_{ox,onset}(M) - E_{MLCT}(M)$ [84,85].

(4) Most of current studies about NIR ECL reports are still limited to explore the new NIR luminophores and their intensities-based bioanalysis applications. Taking into accounts of unique advantages of NIR luminophores in bio-imaging analysis, it deserves to make great efforts to develop NIR luminophores-based ECL imaging in the future though there are still many challenges currently, such as improving the sensitivity of imaging equipment, inherent limitations of ECL reactions, *etc.*

In conclusion, we believe NIR ECL luminophores and their-related applications would achieve more progresses and also inevitably bring new brilliant prospects of the traditional ECL-related analytical technologies in the future.

Declaration of competing interest

The authors declare that they have no known competing financial interests or personal relationships that could have appeared to influence the work reported in this paper.

Acknowledgments

This work was financially supported by Qing Lan Project of Jiangsu Province and Postgraduate Research and Practice Innovation Program of Jiangsu Province (No. KYCX22_3293), Industry-University-Research cooperation project of Jiangsu Province (No. BY20230314), and Industry-University Research Cooperation Prospect Project of Zhangjiagang City (No. ZKYY2203).

Supplementary materials

Supplementary material associated with this article can be found, in the online version, at doi:10.1016/j.cclet.2024.109622.

References

[1] S.K. Lee, M.M. Richter, L. Strekowski, et al., Anal. Chem. 69 (1997) 4126–4133.
[2] A.M. Spehar-Deleze, Y. Pellegrin, T.E. Keyes, et al., Electrochem. commun. 10 (2008) 984–986.
[3] L. Sun, L. Bao, B.R. Hyun, et al., Nano Lett. 9 (2009) 789–793.
[4] K.N. Swanick, M. Hesari, M.S. Workentin, et al., J. Am. Chem. Soc. 134 (2012) 15205–15208.
[5] L. Zhao, X. Song, X. Ren, et al., Anal. Chem. 93 (2021) 8613–8621.
[6] J. Wang, H. Han, Rev. Anal. Chem. 32 (2013) 91–101.
[7] N.E. Tokel, A.J. Bard, J. Am. Chem. Soc. 94 (1972) 2862–2863.
[8] D.R. Deaver, Nature 377 (1995) 758–760.
[9] A. Juris, V. Balzani, F. Barigelletti, et al., Coord. Chem. Rev. 84 (1988) 85–277.
[10] A.M. Spehar-Deleze, Y. Lu, T. Keyes, et al., ECS Trans. 16 (2009) 69.
[11] J.W. Wu, W.J. Mei, Z.H. Yan, et al., J. Electroanal. Chem. 697 (2013) 21–27.
[12] L. D'Alton, P. Nguyen, S. Carrara, et al., Electrochim. Acta 379 (2021) 138117.
[13] M. Majuran, G. Armendariz-Vidales, S. Carrara, et al., ChemPlusChem 85 (2020) 346–352.

[14] Y.Y. Zhou, Y.M. Ding, W. Zhao, et al., Chem. Commun. 57 (2021) 1254–1257.
[15] S. Kwon Lee, A.J. Bard, Anal. Lett. 31 (1998) 2209–2229.
[16] H. Qi, J.J. Teesdale, R.C. Pupillo, et al., J. Am. Chem. Soc. 135 (2013) 13558–13566.
[17] M. Hesari, J.S. Lu, S. Wang, et al., Chem. Commun. 51 (2015) 1081–1084.
[18] R. Ishimatsu, H. Shintaku, Y. Kage, et al., J. Am. Chem. Soc. 141 (2019) 11791–11795.
[19] R.R. Maar, R. Zhang, D.G. Stephens, et al., Angew. Chem. Int. Ed. 58 (2019) 1052–1056.
[20] M.E. Williams, R.W. Murray, Chem. Mater. 10 (1998) 3603–3610.
[21] Y. Song, W. Zhang, S. He, et al., ACS Appl. Mater. Interfaces 11 (2019) 33676–33683.
[22] W. Zhang, Y. Song, S. He, et al., Nanoscale 11 (2019) 20910–20916.
[23] Y. Wang, Y. Li, W. Zhang, et al., Analyst 146 (2021) 3679–3685.
[24] J. Bosson, G.M. Labrador, S. Pascal, et al., Chem. Eur. J. 22 (2016) 18394–18403.
[25] H. Li, A. Wallabregue, C. Adam, et al., J. Phys. Chem. C 121 (2017) 785–792.
[26] S. Voci, R. Duwald, S. Grass, et al., Chem. Sci. 11 (2020) 4508–4515.
[27] H. Li, R. Duwald, S. Pascal, et al., Chem. Commun. 56 (2020) 9771–9774.
[28] R. Jin, C. Zeng, M. Zhou, et al., Chem. Rev. 116 (2016) 10346–10413.
[29] M. Hesari, M.S. Workentin, Z. Ding, Chem. Sci. 5 (2014) 3814–3822.
[30] M. Hesari, M.S. Workentin, Z. Ding, Chem. Eur. J. 20 (2014) 15116–15121.
[31] M. Hesari, Z. Ding, M.S. Workentin, Organometallics 33 (2014) 4888–4892.
[32] M. Hesari, M.S. Workentin, Z. Ding, ACS Nano 8 (2014) 8543–8553.
[33] M. Hesari, Z. Ding, Acc. Chem. Res. 50 (2017) 218–230.
[34] H. Peng, M. Jian, H. Deng, et al., ACS Appl. Mater. Interfaces 9 (2017) 14929–14934.
[35] T. Wang, D. Wang, J.W. Padelford, et al., J. Am. Chem. Soc. 138 (2016) 6380–6383.
[36] J.M. Kim, S. Jeong, J.K. Song, et al., Chem. Commun. 54 (2018) 2838–2841.
[37] H. Peng, Z. Huang, Y. Sheng, et al., Angew. Chem. Int. Ed. 58 (2019) 11691–11694.
[38] L. Yu, Q. Zhang, Q. Kang, et al., Anal. Chem. 92 (2020) 7581–7587.
[39] H. Jia, S. Yu, L. Yang, et al., ACS Appl. Nano Mater. 4 (2021) 2657–2663.
[40] H. Peng, M. Lai, H. Wang, et al., Anal. Chem. 95 (2023) 11106–11112.
[41] Y. Nie, Y. Zhang, W. Cao, et al., Anal. Chem. 95 (2023) 6785–6790.
[42] Y. Zhou, S. Chen, X. Luo, et al., Anal. Chem. 90 (2018) 10024–10030.
[43] Y. Jia, L. Yang, J. Xue, et al., ACS Sens 4 (2019) 1909–1916.
[44] H. Jia, J. Li, L. Yang, et al., Anal. Chem. 94 (2022) 7132–7139.
[45] L. Yu, M. Li, Q. Kang, et al., Biosens. Bioelectron. 176 (2021) 112934.
[46] H. Lv, R. Zhang, S. Cong, et al., Anal. Chem. 94 (2022) 4538–4546.
[47] J. Liu, R. Zhao, X. Wang, et al., Chem. Commun. 56 (2020) 5665–5668.
[48] S. Chen, H. Ma, J.W. Padelford, et al., J. Am. Chem. Soc. 141 (2019) 9603–9609.
[49] L. Fu, X. Gao, S. Dong, et al., Anal. Chem. 93 (2021) 4909–4915.
[50] H. Jia, L. Yang, D. Fan, et al., Sens. Actuators B: Chem. 367 (2022) 132034.
[51] L.L. Chen, L. Zhao, Z.G. Wang, et al., Small 18 (2022) e2104567.
[52] J. Yao, L. Li, P. Li, et al., Nanoscale 9 (2017) 13364–13383.
[53] N. Pradhan, S. Das Adhikari, A. Nag, et al., Angew. Chem. Int. Ed. 56 (2017) 7038–7054.
[54] Z. Ding, B.M. Quinn, S.K. Haram, et al., Science 296 (2002) 1293–1297.
[55] C. Ding, Y. Huang, Z. Shen, et al., Adv. Mater. 33 (2021) e2007768.
[56] S. Xu, J. Cui, L. Wang, Trends Analyt. Chem. 80 (2016) 149–155.
[57] J. Wang, X. Jiang, H. Han, et al., Electrochem. Commun. 13 (2011) 359–362.
[58] J. Wang, H. Han, X. Jiang, et al., Anal. Chem. 84 (2012) 4893–4899.
[59] G.Z. Zou, G.D. Liang, X.L. Zhang, Chem. Commun. 47 (2011) 10115–10117.
[60] G. Liang, L. Shen, G. Zou, et al., Chem. Eur. J. 17 (2011) 10213–10215.
[61] G. Liang, S. Liu, G. Zou, et al., Anal. Chem. 84 (2012) 10645–10649.
[62] G. Zou, X. Tan, X. Long, et al., Anal. Chem. 89 (2017) 13024–13029.
[63] J. Zhou, L. Nie, B. Zhang, et al., Anal. Chem. 90 (2018) 12361–12365.
[64] X. Gao, K. Fu, L. Fu, et al., Biosens. Bioelectron. 150 (2020) 111880.
[65] G.X. Liang, L.L. Li, H.Y. Liu, et al., Chem. Commun. 46 (2010) 2974–2976.
[66] A.J. Stewart, E.J. O'Reilly, R.D. Moriarty, et al., Electrochim. Acta 157 (2015) 8–14.
[67] J. Wang, X. Jiang, Sens. Actuators B: Chem. 207 (2015) 552–555.
[68] J. Wang, X. Jiang, H. Han, Biosens. Bioelectron. 82 (2016) 26–31.
[69] X. Long, X. Tan, Y. He, et al., J. Mater. Chem. C 5 (2017) 12393–12399.
[70] L. Fu, K. Fu, X. Gao, et al., Anal. Chem. 93 (2021) 2160–2165.
[71] Y.T. Yang, Y.Z. Guo, Z.C. Shen, et al., Anal. Chem. 95 (2023) 9314–9322.
[72] J.L. Liu, J.Q. Zhang, Z.L. Tang, et al., Chem. Sci. 10 (2019) 4497–4501.
[73] J. Huan, Q. Liu, A. Fei, et al., Biosens. Bioelectron. 73 (2015) 221–227.
[74] H. Gao, Z. Zhang, Y. Zhang, et al., J. Electroanal. Chem. 886 (2021) 115104.
[75] D. Jiang, M. Wei, X. Du, et al., Biosens. Bioelectron. 200 (2022) 113917.
[76] M. Wei, X. Du, D. Jiang, et al., Biosens. Bioelectron. 236 (2023) 115420.
[77] Z. Zhang, D. Jiang, Q. Song, et al., Biosens. Bioelectron. 238 (2023) 115551.
[78] L. Yang, C.R. De-Jager, J.R. Adsetts, et al., Anal. Chem. 93 (2021) 12409–12416.
[79] Y. Wang, G. Zhao, H. Chi, et al., J. Am. Chem. Soc. 143 (2021) 504–512.
[80] S.Y. Ji, J.B. Pan, H.Z. Wang, et al., CCS Chem. 4 (2021) 3076–3083.
[81] L. Zhao, X. Song, X. Ren, et al., Biosens. Bioelectron. 191 (2021) 113409.
[82] L. Zhao, M. Wang, X. Song, et al., Chem. Eng. J. 434 (2022) 134691.
[83] L. Zhao, X. Song, H. Wang, et al., Chem. Eng. J. 446 (2022) 136912.
[84] W. Guo, H. Ding, C. Gu, et al., J. Am. Chem. Soc. 140 (2018) 15904–15915.
[85] Y. Zhou, Y. Ding, J. Dong, et al., J. Electroanal. Chem. 895 (2021) 115534.